Determinations of $EF\ ^1\Sigma_g^+ \leftarrow X^1\Sigma_g^+$ transition frequencies in H_2, D_2, and HD

A. Yiannopoulou,[1,*] N. Melikechi,[2] S. Gangopadhyay,[3] J. C. Meiners,[4] C. H. Cheng,[5,†] and E. E. Eyler[5]
[1]*Department of Physics and Astronomy, University of Delaware, Newark, Delaware 19716, USA*
[2]*Applied Optics Center and Department of Physics, Delaware State University, Dover, Delaware 19901, USA*
[3]*General Dynamics Advanced Information Systems, 3021 American Blvd. East, Bloomington, Minnesota 55425, USA*
[4]*Physics Department, University of Michigan, Ann Arbor, Michigan 48109, USA*
[5]*Physics Department, University of Connecticut, Storrs, Connecticut 06269, USA*
(Received 14 October 2005; published 9 February 2006)

We have measured the energies of several rotational branches of the (0,0) band of the $EF\ ^1\Sigma_g^+ \leftarrow X^1\Sigma_g^+$ transition in molecular hydrogen by use of Doppler-free two-photon laser excitation at 202 nm. The accuracy for all three stable isotopic variations is 8 parts in 10^9, nominally a fourfold improvement over previously available results, but some of the transition energies differ from previous work by as much as three standard deviations. The improved accuracy derives principally from our ability to measure the optical phase evolution of nanosecond laser pulses, then to predict quantitatively the line shapes of multiphoton transitions excited by them. The results allow comparably accurate determinations of the *EF* state term energies, which in turn help to calibrate the entire excited-state spectrum of this fundamental molecular system. These improved calibrations are particularly useful to recent and ongoing efforts to determine the dissociation energy and ionization potential with improved accuracy.

DOI: 10.1103/PhysRevA.73.022506 PACS number(s): 33.20.Lg, 39.30.+w, 33.15.Ry, 33.15.Fm

I. INTRODUCTION

The $EF\ ^1\Sigma_g^+$ state of molecular hydrogen has played a key role in laser-based experiments because as the lowest excited singlet state of H_2, it is well situated as a platform for multistep excitations. In particular, it has served this purpose in many of the most recent determinations of the ionization potential (IP) and dissociation energy (D_0) [1–5]. Here we describe resonant multiphoton ionization (REMPI) measurements of the *EF* state, with greatly improved accuracy. Previous measurements of the *EF* state were performed by Gilligan and Eyler [3,6], using Doppler-free two-photon excitation with a frequency tripled dye laser. Our new measurements use a similar overall scheme, with many minor improvements and two major changes: (1) We have redesigned the pulsed laser amplifier chain to produce pulses with minimal optical phase excursions and high spatial mode quality; (2) We have added an optical heterodyne setup to directly measure optical phase perturbations, and use these results to numerically model the line shapes of the signals observed.

The historical perspective of this paper is somewhat unusual because much of the experimental work described here was completed several years ago, initially at the University of Delaware and later at the University of Connecticut. Its publication was delayed because of the departure of several of the key research personnel. As a consequence, preliminary versions of our results have already been used to calibrate other measurements [5,7,8]. Additionally, some of the line-shape analysis techniques originally developed for this work have subsequently been used to analyze the 1^1S-2^1S transition in atomic helium [9], and have been further developed for other applications [10]. Here we focus on aspects of the experiment that are not described in these existing publications, and on the physical and mathematical modeling required to obtain accurate values for the transition energies.

Although numerous issues of calibration and systematic shifts must be addressed in such a measurement, there are two principal issues that required innovative approaches: residual Doppler shifts due to angular alignment between the input beam and the counterpropagating beam, and optical phase perturbations in the uv laser pulse caused by pulsed laser amplification and nonlinear frequency mixing. The angular alignment issue was solved by careful optical design, but the optical phase perturbations are the largest single error source, requiring careful measurement and line-shape modeling as described below. The result is quite gratifying—we have observed REMPI transitions with linewidths very close to the Fourier-transform limit set by the laser pulse duration, and have measured the transition frequencies to an accuracy of 25 MHz. The fractional accuracy of 8×10^{-9} is among the best ever achieved for far-uv spectroscopy, and is similar to the accuracy reported for recent measurements of transitions in atomic helium [9,11]. This accuracy is somewhat better than has been attainable for one-photon VUV transitions in other species such as neon [12] and CO [13], or for direct one-photon excitation of other states in H_2 [14,15].

II. EXPERIMENT

The overall configuration for exciting $EF \leftarrow X$ transitions in molecular hydrogen is illustrated in Fig. 1. As shown in

*Present address: lycee "Saint Thomas D'Aquin Veritas," 56 rue du Perron, 69600 Oullins, France.
†Present address: Panasonic Boston Laboratory, 68 Rogers St., Cambridge, MA 02142, USA.

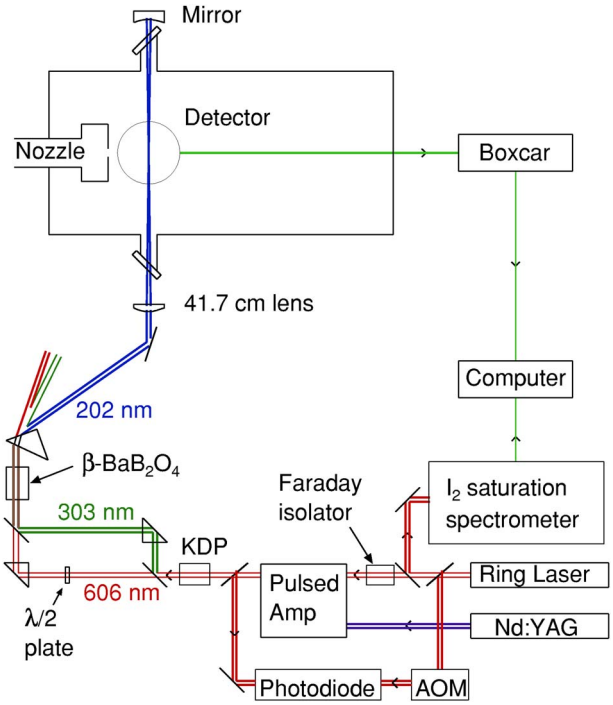

FIG. 1. (Color online) Experimental scheme for measurement of two-photon $EF \leftarrow X$ transitions. The acousto-optic modulator (AOM) and photodiode are used for an optical heterodyne analysis of the pulsed amplifier output.

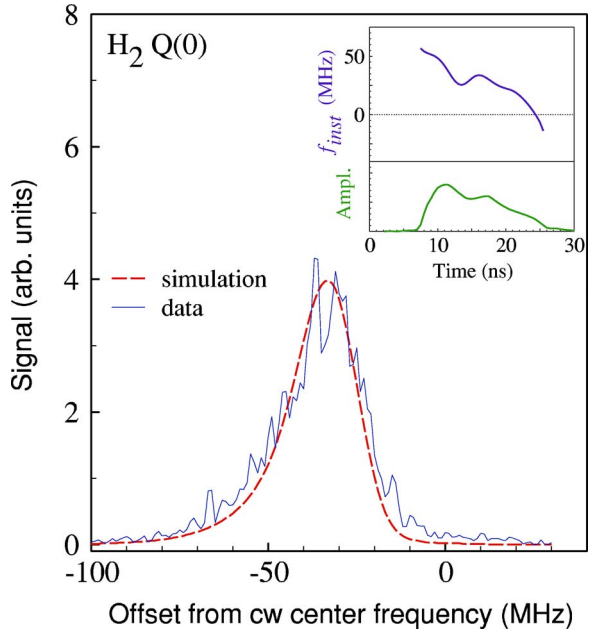

FIG. 2. (Color online) Typical spectrum using strongly chirped laser pulses. Shown is the $Q(0)$ branch for H_2. Profiles of the laser amplitude and instantaneous frequency evolution are shown in the inset. The solid line is a model line shape based on the measured frequency evolution, as described in Sec. III.

the figure, a pulsed supersonic beam of hydrogen is intersected at right angles by a pair of counterpropagating laser beams at 202 nm, providing Doppler-free excitation. We generate the required 202 nm laser pulses by frequency tripling of pulse-amplified 606 nm laser radiation as described below. We detect the transitions using REMPI: a third photon at the same wavelength ionizes a fraction of the excited-state molecules, which are detected by time-of-flight mass spectroscopy with a discrete-dynode multiplier or microsphere plate detector.

A. Pulsed amplification and chirp reduction

To obtain laser pulses at 606 nm combining high peak power with bandwidths closely approach the Fourier-transform limit, we amplify the output of a single-mode cw ring dye laser, Coherent CR 699-21, in a Nd:YAG-pumped (YAG denotes yttrium aluminum garnet) three-stage amplifier. The pulsed amplifier is identical to the one described in Ref. [16]. It uses a series of Bethune-type dye cells [17] to produce output pulses about 10 nsec in duration with energies of a few mJ when pumped by 100 mJ pulses from an excimer or Nd:YAG laser.

We use an optical heterodyne scheme to explicitly measure the temporal evolution of the instantaneous frequency of the nanosecond laser pulse, which is perturbed by the time-changing susceptibility of the laser dye. The experimental setup and phase extraction algorithm have been described previously [18], and are elaborations of a scheme originally developed by Fee, Danzmann, and Chu [19]. In brief, we measure the beat note of the pulsed laser against a frequency-shifted sample of the cw laser, then use Fourier-domain analysis to extract the instantaneous frequency,

$$f_{inst} = \frac{1}{2\pi}\frac{d\phi}{dt}. \quad (1)$$

For our initial attempts at this measurement we used excimer-pumped Rhodamine 610 dye, which provided ample energy, but with a strongly chirped frequency profile as shown in the inset of Fig. 2. The chirp was probably aggravated because we used a transversely pumped dye cell for the first stage, as in the earlier work of Ref. [3]. Although we did not use this data set for our final results because of potential problems due to angular misalignment that are described below, it served as a very useful cross check on our ability to measure and correct for optical phase perturbations.

For the final data set, we switched to an injection-seeded Nd:YAG laser pump, Continuum model YG681, which provided a smoother temporal profile. More importantly, we generated "chirp-controlled" pulses obtained by using a customized laser dye mix as described in Refs. [16,20]. We carefully prepared a mix of Rhodamine 610 and DCM laser dyes such that the real part of the linear susceptibility is zero at the design wavelength. By this method the frequency chirp can be reduced by more than an order of magnitude, as shown in the inset of Fig. 3. In this final configuration the amplifier chain typically produced 3.5 mJ pulses at 606 nm, 8.5 ns in duration.

The evolution of the instantaneous frequency of the amplified pulses was uniform across the beam profile and reproducible over a time scale of hours to within 2–3 MHz. How-

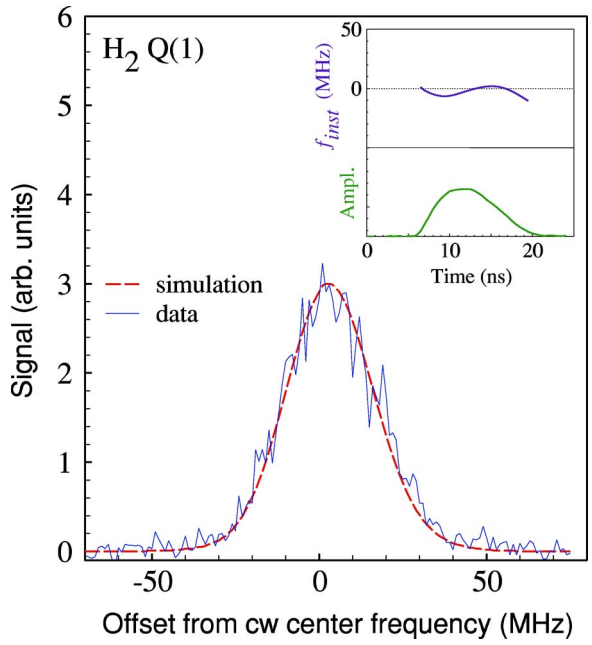

FIG. 3. (Color online) Typical spectrum using chirp-controlled laser pulses. Shown is the $Q(1)$ branch of H_2. All other information is the same as given in Fig. 2.

ever, we found that we had to change the dye about once a day to maintain pulses with minimal chirping. As the dye ages, substantially more chirping of the laser frequency occurs, degrading our ability to measure and correct for optical phase perturbations.

B. Frequency tripling

The required 202 nm radiation is generated by frequency tripling the 606 nm pulses using the same scheme as [3]. In brief, the pulsed 606 nm laser radiation is frequency-doubled in a nonlinear potassium dihydrogen phosphate (KDP) crystal, then the 303 nm harmonic radiation is mixed with the residual 606 nm radiation in a β-BaB_2O_4 (BBO) crystal. The typical second-harmonic energy was approximately 300 μJ per pulse, corresponding to a conversion efficiency of about 20%, and the third-harmonic energy was about 120 μJ.

Complications can arise in the third-harmonic generation because additional optical phase distortions can be introduced by nonlinear mixing [21]. We discuss this problem in more detail in Sec. III. In brief, when phase matching is imperfect because of beam walkoff or improper angle tuning, the instantaneous frequency profile undergoes dispersion-shaped excursions during the duration of the laser pulse, because of nonlinear coupling between the fundamental beam and its out-of-phase second harmonic.

To ensure that the entire fundamental beam is phase-matched, we designed our mixing scheme so that the confocal parameter z_0 is much larger than the crystal length. The beam diameter in the crystal was about 400 μm, corresponding to z_0=83 cm. Care was taken to collimate the input beams and to optimize the angle tuning of both the doubling and tripling crystals before each spectrum was recorded.

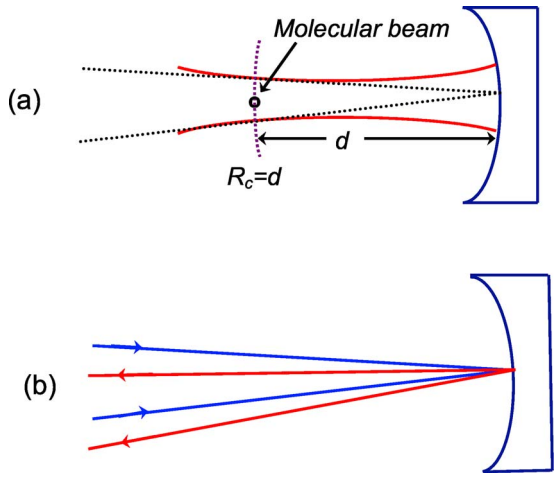

FIG. 4. (Color online) Scheme for canceling errors due to angular misalignment. Part (a) shows the geometry of the counterpropagating beam, and part (b) shows ray trajectories if the mirror undergoes a small angular displacement.

C. Counterpropagating beams: diffractive cancellation of angular misalignment

In our initial attempts using the excimer-pumped pulsed amplifier, we simply focused the 202 nm beam to a waist at the position of the molecular beam, using a lens of 41.7 cm focal length, then counterpropagated the beam using a plane-parallel mirror and an additional lens. Unfortunately we discovered a potential systematic error while completing our analysis of the results: if there is angular misalignment between the two 202 nm beams, a significant residual Doppler shift can result. If one laser beam is accurately perpendicular to the molecular beam, and the other is displaced by an angle δ, the transition frequency ω will be shifted by an amount

$$\frac{\Delta\omega}{\omega} = 2\frac{v}{c}\sin(\delta/2), \tag{2}$$

where v is the speed of the molecular beam. Under our conditions, we found that a plausible misalignment could result in a worst-case shift of up to 60 MHz, or 0.002 cm^{-1}, in the full two-photon transition energy.

It was for this reason that we undertook a completely separate new set of measurements, used to determine the final results reported here. However, this also provided an opportunity to switch to the chirp-controlled pulses described above, which yielded substantial additional benefits in the attainable accuracy.

In our new configuration, we designed the optics such that diffractive wavefront curvature cancels the effects of minor angular misalignment, at least for a laser with a perfect Gaussian TEM_{00} transverse mode. The geometry is shown in Fig. 4. A concave mirror provides the counterpropagating beam, and is adjusted so the two beams have identical waists. The molecular beam is positioned away from the waist, at a position where the wavefront curvature radius is equal to the distance to the mirror. At this point, every **k** vector intersects the center of the mirror, as illustrated by the two tangent lines drawn in Fig. 4. It follows that if the angle

of the mirror is shifted slightly as sketched in Fig. 4(b), each counterpropagating ray will still be precisely antiparallel to the coinciding incoming ray at the position of the molecular beam.

In our experiment the counterpropagating beam is provided by reflection from a curved dielectric mirror with a focal length of 15.5 cm, placed 75 cm from the input lens. With this configuration the waists of both beams coincide, with a transverse $1/e^2$ radius of approximately $\omega_0=76$ μm. At the position of the molecular beam, the transverse radius increases to approximately 300 μm. The corresponding laser irradiance for the highest 202 nm pulse energies used in this work, about 100 μJ, is about 7 MW/cm^2.

Unfortunately the spatial mode of our 202 nm beam was of rather poor quality. To account for possible partial failures of the cancellation scheme, we empirically measured the effects of angular misalignment as described in Sec. IV. Major misalignments produced shifts of up to 9 MHz in the full two-photon transition energies, which was not as good as we had hoped, but still far better than for the original configuration.

D. Wavelength measurements

Optical frequency calibration is performed using Doppler-free saturated absorption spectroscopy, with the same iodine cell used previously by [3], in much the same configuration. The cw laser wavelength is measured by comparison to iodine lines that are known with an accuracy of 250 kHz [6]. To measure the frequency interval between the molecular resonances and the closest iodine hyperfine lines, we used marker fringes from a 25 cm confocal Fabry-Perot interferometer (Burleigh CF 25) which was temperature stabilized to 0.03 C. To reduce the noise due to fluctuations from the dye laser, the signals from the interferometer as well as the iodine absorption spectrum are normalized by the laser intensity.

E. Spectra

The REMPI signal resulting from three-photon ionization is observed using the same scheme as [3], with the minor exception that in much of the work a microchannel plate detector is used rather than a photomultiplier. Details are given in Refs. [3,21,22]. The experiment is carried out in a collimated molecular beam produced by a supersonic pulsed valve. Signal ions are accelerated towards the detector by a small dc electric field, which we varied between 20 and 55 V/cm to verify that there were no detectable dc Stark shifts in the transition frequencies.

Figure 5 shows a typical spectral scan. In each spectrum we simultaneously recorded the REMPI signal, iodine lines, marker interferometer etalon fringes, and diagnostic signals from the wavemeter of the cw dye laser. The laser pulse energy at 202 nm was measured before and after each scan with a pyroelectric energy meter (Gentec model ED 100-A). We also periodically recorded heterodyne beats for the pulsed 606 nm light, typically sampling sets of 50 successive laser shots so that averaging can be used to reduce the noise level.

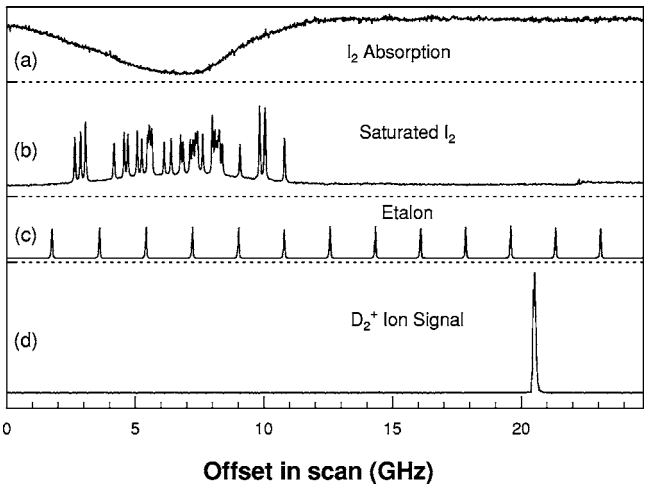

FIG. 5. Spectral scan over the $Q(1)$ line in D_2, showing iodine reference spectra and marker fringes from a confocal interferometer. The offset frequency refers to the full two-photon $EF \leftarrow X$ transition energy in trace (d). Traces (a)–(c) are obtained directly with the 606 nm cw laser, which scans only $\frac{1}{6}$ as rapidly. Thus the marker fringes in (c), from a 300 MHz interferometer, are separated by 1.8 GHz.

III. LINE-SHAPE MODELING

In this section, we discuss details of the numerical model developed to predict the line shape of the REMPI signal. The measured frequency chirp of the pulse-amplified laser is used as input to a model that includes phase distortions of the pulse-amplified beam and resonant two-photon absorption, three photon ionization. Other contributions to the line shape are negligible, because the experiment is carried out under Doppler-free and collision-free conditions, and the natural linewidth is about 200 times smaller than the laser-limited linewidth. Thus, the model line shape can be directly compared to the experimental spectra.

The starting point is to reconstruct the electric field of the amplified pulse from the optical heterodyne measurements, including both its amplitude $E_\omega(t)$ and its phase $\phi(t)$,

$$\mathbf{E}_\omega(t) = |\mathbf{E}_\omega(t)|\exp[i\varphi(t)]. \tag{3}$$

The electric field of the frequency-tripled light is then calculated by assuming a simple power-law dependence on the field of the fundamental beam,

$$\mathbf{E}_{3\omega}(t) = [\mathbf{E}_\omega(t)]^p, \tag{4}$$

where the exponent $p \simeq 2.3$ is experimentally determined. In the limit of very low irradiance an exponent of 3.0 would be expected because tripling is intrinsically a third-order process. This expression is approximate not only because of partial saturation in the harmonic conversion process, but also because, in the presence of walk-off and imperfect phase matching, the harmonic field can acquire phase distortions due to nonlinear coupling with the fundamental [21,23,24]. We minimize these effects by careful design and phase matching, and we determine a limit on the associated errors in Sec. IV below.

The probability of two-photon absorption induced by two counterpropagating beams with a relative delay of Δt is proportional to the squared magnitude of the product of the fields,

$$P_{TPA}(t) \propto |\mathbf{E}_{3\omega}(t)\mathbf{E}_{3\omega}(t-\Delta t)|^2. \quad (5)$$

To calculate the REMPI signal we must also include the photoionization step. We introduce it in a somewhat *ad hoc* fashion as a completely independent process,

$$P_{\mathrm{REMPI}}(t) \propto |\mathbf{E}_{3\omega}(t)\mathbf{E}_{3\omega}(t-\Delta t)|^2 P_{ion}(t). \quad (6)$$

Here the ionization probability $P_{ion}(t)$ for an EF state molecule produced at time t is proportional to the integrated irradiance of the subsequent portion of the laser pulse,

$$P_{ion}(t) \propto \int_t^\infty |\mathbf{E}_{3\omega}(t') + R\mathbf{E}_{3\omega}(t'-\Delta t)|^2 dt', \quad (7)$$

and R is a factor that accounts for losses in the counterpropagating beam due to mirror reflectance and window transmission. In this experiment R was measured to be approximately 0.75. The frequency-domain line shape of the REMPI signal is found by transforming Eq. (6),

$$\Gamma(\omega) \propto |\mathcal{F}[\mathbf{E}_{3\omega}(t)\mathbf{E}_{3\omega}(t-\Delta t)[P_{ion}(t)]^{1/2}]|^2, \quad (8)$$

where $\mathcal{F}$ denotes the Fourier transform.

This predicts a cubic dependence of the signal on the uv beam irradiance. Experimentally we observed a dependence just slightly less than this, with a power-law exponent between 2.6 and 2.8. As a result, we can expect that this model provides a reasonably accurate description. Nevertheless it is somewhat simplistic in two regards: First, we oversimplify the REMPI process as an unsaturated two-step process, with a two-photon excitation step followed by a separate photoionization step, and second, we neglect line broadening effects due to power broadening, initial-state depletion, or saturation. In the following section we will discuss the uncertainties associated with these omissions. We also neglect the effects of standing wave formation by the counterpropagating uv beams, which are not expected to be important apart from the fact that intensity-dependent effects should actually be interpreted as averages over the very small spatial period (100 nm) between adjacent antinodes.

To determine the experimental transition frequencies, we perform a direct least-squares fit of this model line shape to the experimental signal. Only two adjustable fitting parameters are needed: the transition frequency and the amplitude. In Figs. 2 and 3, the solid lines show typical results for the line-shape modeling, for the cases of a strongly chirped pulse and a chirp-compensated pulse. The match with observed line shapes is quite good, especially for the chirp-compensated pulse, with the exception of the outer wings of the transition.

Accuracy of the model

The uncertainties associated with our line-shape modeling arise at three different stages: uncertainties in determining the optical phase evolution of the 606 nm laser pulses, errors in determining the corresponding evolution of the third-harmonic pulse at 202 nm, and errors due to imperfect physical modeling of the line shape. Here we discuss each in turn. In this section, all frequencies are expressed relative to the full two-photon transition energy, not to the cw laser beam whose 606 nm wavelength corresponds to $\frac{1}{6}$ of this interval.

TABLE I. Uncertainty budget for a typical $EF \leftarrow X$ transition. Contributions are primarily due to potential systematic errors, with the exception of numerical noise, ac Stark extrapolation, and statistics. However, many of these systematic effects are expected to vary randomly from run to run.

Category	Description	Size (MHz)
Doppler	Angular misalignment	5
Chirp	Numerical reconstruction	12
Chirp	Laser fluctuations	6
Chirp	Numerical noise	1.2
Chirp	Third harmonic generation	6
Lineshape	Model physics	15
Lineshape	All other	3
Molecular	ac Stark extrapolation	5
Molecular	dc Stark shifts	< 3
Metrology	Scan linearization	6
Metrology	Interferometer thermal drift	6
Metrology	Statistics, data granularity	5
Metrology	Wavelength calibration	< 1
Quadrature sum		25

There are both random and systematic uncertainties in extracting the optical phase evolution of the pulse-amplified 606 nm laser from optical heterodyne beats, as discussed in a recent review of the subject [10]. We estimated the associated uncertainties by performing numerical "experiments" using synthetic heterodyne beats calculated using realistic laser pulse envelopes and chirp profiles, optionally incorporating random noise as well. By comparing the results of our phase reconstruction algorithms with the input data, we could determine the errors, both due to systematic limitations and to random fluctuations. We could also assess the effects of empirical limitations, such as the need to exclude from our analysis the low-intensity tails of the pulse, where numerical noise becomes excessive. Full details are provided in the Ph.D. thesis of Gangopadyay [21]. For the chirp-compensated laser pulses used in our final measurements, the uncertainties in the $EF \leftarrow X$ transition energies are dominated by effects of the numerical chirp reconstruction error (12 MHz), laser fluctuations (6 MHz), and numerical noise (1.2 MHz). In Table I we tabulate these uncertainties together with all other significant contributions to the overall uncertainty budget.

Next we consider uncertainties associated with optical third-harmonic generation of our 15–20 ns laser pulses, caused by deviations from the simple power-law dependence of Eq. (4). It has been shown theoretically [23,24] and experimentally [21] that in an imperfectly phase-matched nonlinear crystal, the mismatch between the input fields and the

generated fields causes perturbations to both, yielding a roughly dispersion-shaped distortion in the instantaneous frequency profile. The frequency excursions in second-harmonic generation can easily reach 25 MHz, which would correspond to 75 MHz in the full $EF \leftarrow X$ transition energies. Fortunately the shifts on the leading edge of the pulse partially cancel those on the falling edge, and the maximum extent of the shifts can be reduced to the sub-MHz level by careful phase matching and by reducing the irradiance using relatively large beam sizes. We took full advantage of the knowledge gained in Ref. [21] in designing our experiment. No obvious effects of the harmonic generation on the line shape were observed unless we intentionally detuned the angle matching of the nonlinear crystals, in which case minor line-shape distortions were observed.

Because we had no way to directly measure phase perturbations in the 202 nm radiation, we instead set a limit by repeating most of our measurements at several different laser powers, and extrapolating to the zero-power limit in which no shifts can occur. To separate the effects of ac Stark shifts of the hydrogen lines from those of the third-harmonic generation process, we used two different attenuation schemes. The first method, using only neutral density (ND) filters in the 202 nm beam, affected only the ac Stark shift, while the second method, in which we attenuated the 606 nm pulses by reducing the pump energy to the final amplifier cell, affected both the third-harmonic generation and the ac Stark effect. By looking at the difference between the two sets of results, we can set a bound on errors arising in the third-harmonic generation process.

We were able to use both extrapolation methods for six of the seven transitions measured in this paper. The mean of the differences between the extrapolations using amplifier blocking and ND filter blocking was just 1.8 MHz, much smaller than the 16 MHz average magnitude of the differences, which arises largely from random variations from one measurement to another. Thus we estimate that the error associated with phase perturbations introduced during frequency tripling is probably only about 2 MHz, although we have chosen to use a conservative estimate of 6 MHz in the error budget of Table I because of our inability to directly measure optical phase perturbations at 202 nm. We also estimated the uncertainty associated with an imperfect knowledge of the exponent p in Eq. (4), by allowing it to vary between 2 and 3 in our line-shape modeling. This variation affects the results for the transition frequencies by much less than 1 MHz, and can safely be neglected.

Finally, we consider the effects of imperfect physical modeling of the line shape. Extensive tests were performed to evaluate the accuracy of the model of Eqs. (7) and (8), including its sensitivity both to the underlying physical assumptions and the input parameters. Again, full details appear in Ref. [21]. Our numerical experiments included changing the relative delay time Δt between the two counterpropagating beams, assuming that the ionization process is instantaneous rather than stepwise, considering the effects of the possible saturation of the different processes (two-photon excitation and ionization), changing the relative strength of the counterpropagating beams by changing the value of R, and checking for the effects of noise on the spectrum. We varied each of the experimental parameters over a range approximately equal to its experimental uncertainty.

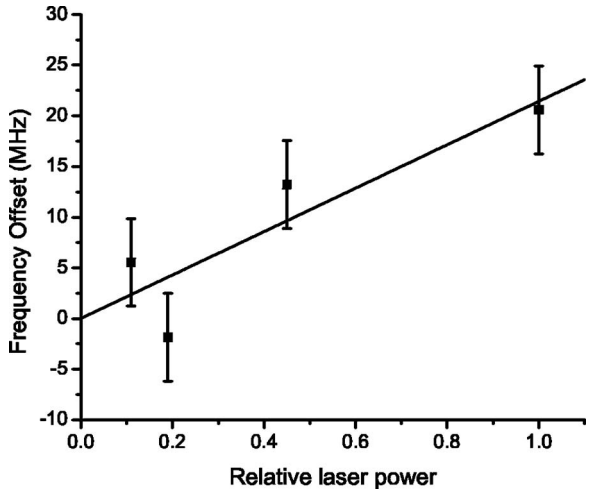

FIG. 6. Transition frequency as a function of pulse energy of the third harmonic, attenuated using ND filters. The ac Stark shift is roughly 20 MHz/(MW/cm^2).

The largest effects are due to modifications in the physical modeling of the ionization step. For example, if we assume the extreme limit of instantaneous ionization, where $P_{ion}(t) = 1$ in Eq. (6), the modeled transition frequency for a measurement with a typical chirp-compensated laser pulse shifts by approximately 15 MHz. However, we note that this would also result in an excess linewidth of about 50% compared to the observed signals, and it would result in a quadratic power law for the dependence of the signal on the uv power, far from the observed power law of about 2.6. It is somewhat harder to determine the effects of other saturation or depletion effects in Eq. (6), since this requires rather arbitrary assumptions about the exact form of the broadening. However, we performed a variety of checks that suggest the associated uncertainties do not much exceed 6 MHz. As a conservative limit, we assume a systematic uncertainty of 15 MHz due to an imperfect modeling of the REMPI process. The quadrature sum of all of the other model-dependent uncertainties is just 3 MHz, and contributes little to the overall uncertainty budget.

IV. ANALYSIS AND RESULTS

The $EF \leftarrow X$ line centers are found by fitting the experimental data with the results of the line-shape model described in Sec. III. To obtain the actual transition energies a few additional steps are required to account for systematic shifts not included in the modeling.

The most important of these is to account for systematic shifts due to the ac Stark effect. As mentioned above in Sec. III, we use neutral density filters to attenuate the 202 nm laser power, and linearly extrapolate the transition frequency to the zero-power value. One such power extrapolation is shown in Fig. 6. The Stark slopes vary considerably from one transition to another, although the overall scale of the shifts is typically a few tens of MHz per MW/cm^2 of laser

irradiance. In the uncertainty budget we included a contribution of 5 MHz for the typical uncertainty of the power extrapolation, although in a few cases the actual statistical uncertainty of the linear fits was considerably better than this.

We also made tests for systematic shifts due to the dc Stark effect and residual shifts due to angular misalignment of the 202 nm beams. We observe no measurable dc Stark shifts while increasing the dc field in the interaction region from 20 V/cm to 55 V/cm. This establishes an upper of 3 MHz for dc Stark shifts, in accord with rough perturbation-theory estimates indicating that these shifts should be negligible. For angular misalignment, we set a limit by intentionally severely misaligning the counterpropagating beam to reduce the signal size by half. The largest observed shift in the transition frequency was 9 MHz, and in Table I we have conservatively included an uncertainty of 5 MHz.

In the overall uncertainty budget shown in Table I, most entries are applicable to all seven of the measured transitions. Two exceptions are the contributions from etalon thermal drift and scan linearization, which vary considerably because they depend on the separation between the molecular hydrogen resonance and the nearest iodine reference line. Nevertheless, because the largest contributions are essentially the same for all seven transitions, the uncertainties of the final results are nearly identical. This 25 MHz uncertainty is the quadrature sum of the individual contributions, which is appropriate because no correlation is expected between any of the various contributions, including the systematic contributions.

It is informative to compare these final results with those obtained from our initial attempts using the strongly chirped pulses shown in Fig. 2. A full analysis of the initial data set is carried out in the thesis of Meiners [22]. Despite the much larger frequency chirp, and the potential for uncontrolled errors up to 60 MHz arising from angular misalignment of the counterpropagating 202 nm beams, the results are in remarkable agreement. The rms deviation between the two sets of measurements is just 10.4 MHz, well within the estimated error bars of either set of measurements taken alone. This does much to inspire confidence in our ability to measure and compensate for laser frequency chirping. It also suggests that the actual errors due to angular misalignment are much smaller than the upper bound, but because this cannot actually be proven, we use only the final data set taken with chirp-controlled pulses to determine the results reported here.

Table II gives a summary of the experimental results, together with the most recent previous determinations, based on earlier work from our own group [3,6]. We note that the absolute term energies of the *EF* state can be obtained with comparable accuracy by combining the results from Table II with accurate calculations of the *X* state rotational energy levels, such as those in Ref. [8].

It is evident from Table II that our new measurements disagree significantly with the earlier experiments. In each case the new measurements are shifted to higher frequencies, by amounts ranging from 1.6 to 3.5 standard deviations in the combined uncertainties. We are fairly certain that the explanation lies in our failure to quantitatively measure the laser chirp in the work of Ref. [3], in which the only allowance for optical phase perturbations was to use an interferometer to crudely set a limit on the average frequency shift of the pulse-amplified 606 nm light. If we assume that the laser frequency profiles looked similar to the chirped pulse shown in Fig. 2, the corresponding transition energies would have been too low by roughly 25 MHz multiplied by six (for a two-photon transition with a third-harmonic radiation). This corresponds to an error of 0.005 cm^{-1}, in good agreement with the third column of Table II.

TABLE II. Frequencies for the (0,0) band of the $EF \leftarrow X$ transition, in cm^{-1}, and comparisons with the most accurate previous results.

Transition	This work	Previous value, Ref. [6]	Difference
H_2 $Q(0)$	99164.7871(8)	99164.782(3)	0.005(3)
H_2 $Q(1)$	99109.7316(8)	99109.727(3)	0.005(3)
HD $Q(0)$	99301.3461(8)	99301.340(3)	0.006(3)
HD $Q(1)$	99259.9184(8)	99259.912(3)	0.006(3)
D_2 $Q(0)$	99461.4490(8)	99461.440(3)	0.009(3)
D_2 $Q(1)$	99433.7166(8)	99433.710(3)	0.007(3)
D_2 $Q(2)$	99378.3937(8)	99378.387(2)	0.007(2)

We have learned that an independent remeasurement of $EF \leftarrow X$ transitions is being conducted by the group of Wim Ubachs [25]. Their experimental scheme is somewhat different, relying on the fourth-harmonic generation from an 808 nm laser and calibration with a femtosecond frequency comb. Their preliminary results are reported to be in reasonable agreement with the results reported here.

Relation to measurements of the dissociation energy (D_0) and ionization potential

The *EF* state transition energies reported here are essential to our ongoing effort to redetermine the ionization potential of molecular hydrogen to an accuracy of 0.001 cm^{-1}. The planned experiment relies on measurements of transitions from the *EF* state to high Rydberg states whose binding energy relative to the ionization limit can be determined very accurately.

The impact on existing determinations of the IP and the dissociation energy is more modest, because the required revisions are in all cases less than the total estimated uncertainties. Additionally, in the case of the dissociation energy, the results reported here were already incorporated in a recent measurement by our own group [5].

In the case of the IP, some previously published results should be slightly modified. For example, in the case of the HD isotope our own earlier result of 1 245 658.481(12) cm^{-1} should be updated to 1 245 658.487(12) cm^{-1}. This brings the result extremely close to a recent redetermination [14] that used a completely independent calibration technique to obtain a result of 124 568.491(17) cm^{-1}. However, the statis-

tical significance of this revision is minimal, so one cannot really argue that the agreement is improved meaningfully. The same is true of the other isotopic variants: any IP determinations that relied on Ref. [6] *EF* state should be increased by the amounts indicated in Table II, although the adjustments are always smaller than the overall uncertainties. We note that in two recent publications regarding the IP [7,8], the preliminary results listed in Ref. [22] were used, and they differ by no more than 30 MHz from the final results in Table II.

V. CONCLUSIONS

We have reported significantly improved measurements of the *EF* state energy levels of molecular hydrogen and its isotopomers, using Doppler-free two-photon laser spectroscopy with a carefully optimized pulse-amplified laser. The phase evolution of the pulse was measured by optical heterodyne methods and was used to model the line shapes of the $EF \leftarrow X$ transitions. The agreement between the predicted and observed line shapes is excellent apart from slight discrepancies in the far wings. The absolute accuracy of the two-photon transition frequencies is 8 parts in 10^9, one of the most accurate measurements performed to date using pulsed lasers. Previous results in Refs. [3,6] differ by as much as three standard deviations, and the discrepancies are almost certainly due to failure to adequately account for strong frequency chirping of the pulse-amplified laser used in the earlier work. Our new results set a benchmark for calibrating the remainder of the excited-state spectrum of molecular hydrogen. More significantly, they serve to calibrate the intermediate states used in recent and ongoing determinations of the IP and dissociation energy.

ACKNOWLEDGMENTS

This research was supported by the National Science Foundation and by the University of Connecticut.

[1] C. Jungen, I. Dabrowski, G. Herzberg, and M. Vervloet, J. Chem. Phys. **93**, 2289 (1990).
[2] C. Jungen, I. Dabrowski, G. Herzberg, and M. Vervloet, J. Mol. Spectrosc. **153**, 11 (1992).
[3] J. M. Gilligan and E. E. Eyler, Phys. Rev. A **46**, 3676 (1992).
[4] E. E. Eyler and N. Melikechi, Phys. Rev. A **48**, R18 (1993).
[5] Y. P. Zhang, C. H. Cheng, J. T. Kim, J. Stanojevic, and E. E. Eyler, Phys. Rev. Lett. **92**, 203003 (2004).
[6] D. Shiner, J. M. Gilligan, B. M. Cook, and W. Lichten, Phys. Rev. A **47**, 4042 (1993).
[7] A. de Lange, E. Reinhold, and W. Ubachs, Phys. Rev. A **65**, 064501 (2002).
[8] L. Wolniewicz, J. Chem. Phys. **103**, 1792 (1995).
[9] S. D. Bergeson, *et al.*, Phys. Rev. Lett. **80**, 3475 (1998); also S. D. Bergeson, *et al.*, J. Opt. Soc. Am. B **17**, 1599 (2000).
[10] R. T. White, Y. He, B. J. Orr, M. Kono, and K. G. H. Baldwin, J. Opt. Soc. Am. B **21**, 1577 (2004).
[11] K. S. E. Eikema, W. Ubachs, W. Vassen, and W. Hogervorst, Phys. Rev. Lett. **76**, 1216 (1996); also Phys. Rev. A **55**, 1866 (1997).
[12] K. S. E. Eikema, W. Ubachs, and W. Hogervorst, Phys. Rev. A **49**, 803 (1994).
[13] W. Ubachs, K. S. E. Eikema, and W. Hogervorst, J. Opt. Soc. Am. B **14**, 2469 (1997).
[14] G. M. Greetham, U. Hollenstein, R. Seiler, W. Ubachs, and F. Merkt, Phys. Chem. Chem. Phys. **5**, 2528 (2003).
[15] W. Ubachs and E. Reinhold, Phys. Rev. Lett. **92**, 101302 (2004).
[16] E. E. Eyler, A. Yiannopoulou, S. Gangopadhyay, and N. Melikechi, Opt. Lett. **22**, 49 (1997).
[17] D. S. Bethune, Appl. Opt. **20**, 1897 (1981).
[18] S. Gangopadhyay, N. Melikechi, and E. E. Eyler, J. Opt. Soc. Am. B **11**, 231 (1994).
[19] M. S. Fee, K. Danzmann, and S. Chu, Phys. Rev. A **45**, 4911 (1992).
[20] N. Melikechi, S. Gangopadhyay, and E. E. Eyler, J. Opt. Soc. Am. B **11**, 2402 (1994).
[21] S. Gangopadhyay, Ph.D. thesis, University of Delaware, 1995 (unpublished).
[22] J. C. Meiners, M.S. thesis, University of Delaware, 1994 (unpublished).
[23] A. V. Smith and M. S. Bowers, J. Opt. Soc. Am. B **12**, 49 (1995).
[24] J.-M. R. Thomas and J.-P. E. Taran, Opt. Commun. **4**, 329 (1972).
[25] W. Ubachs (private communication).